Response of tropospheric water vapor and temperature to El Niño warming in four NCAR models

Tao Zhang and De-Zheng Sun

CIRES/Climate Diagnostics Center

&NOAA/Earth System Research Laboratory

Boulder, Colorado

E-mail: tao.zhang@noaa.gov

April 5, 2007

(Submitted to *Journal of Climate)*

(Revised)

Abstract

To diagnose the causes of an excessive response of the clear-sky greenhouse effect to El Niño warming in the NCAR models, the response of both water vapor and temperature to El Niño warming in the models is examined as a function of height. The percentage response of water vapor to El Niño warming in the models is considerably stronger than the response in the NCEP reanalysis in the middle and upper troposphere (700mb-300mb). The maximum discrepancy with NCEP data at 500 mb reaches 18%/K in CAM3 at T42 and T85 resolution. The discrepancy in the temperature response between the models and NCEP data at all tropospheric levels is within 0.3 K/K, with the maximum discrepancy occurring in the immediate neighborhood of 600 mb. The comparison between the models and ERA-40 reanalysis leads to the similar results.

Employing a radiative model, we have calculated the contributions of the excessive water vapor response in the middle and upper troposphere as well as the contributions from the differences in the lapse rate response to the discrepancies seen in the clear-sky greenhouse effect. The results confirm that the main cause of the excessive response of the clear-sky greenhouse effect is an excessive response of water vapor in the middle and upper troposphere. The excessive response of upper tropospheric water vapor is found to be companied with an excessive response in the cloud cover and vertical motion. Biases in both phases of ENSO contribute to these excessive responses to ENSO.

1. Introduction

Water vapor is the major contributor to Earth's greenhouse effect (Kiehl and Trenberth 1997). The response of the climate system to an increase in the greenhouse gases depends on the feedback of water vapor (Houghton et al. 2001). As we increasingly rely on climate models to assess and predict climate change, we need to know how well our models simulate the water vapor feedback (Stocker et al. 2001, Sun et al. 2001).

The response of water vapor to El Niño warming stands as a useful test bed to isolate and fix potential errors in our simulations of water vapor feedback. This is because the signal is strong, planetary in spatial scale, and has a time scale on which we have good observations. Earlier studies have stressed that El Niño warming is not a good surrogate for global warming because the latter may have a different spatial pattern of warming (Sun and Held 1996 and others). This argument has given back some ground recently as more and more climate models predict El Niño-like warming in response to increases in the greenhouse gases (Meehl and Washington 1996; Timmerman et al. 1999; Cai and Whetton 2000; Boer et al. 2004). Exactly how the climate system responds to anthropogenic forcing may take some time to answer. Fortunately, the need to document carefully and understand the discrepancies between model simulated response of the greenhouse effect of water vapor and that indicated in available observations does not depend much on the answer to this question.

In an earlier study of water vapor feedback in the NCAR CCM3, Sun et al. (2003) found that the response of the clear-sky greenhouse effect to El Niño warming in the model is considerably larger than that indicated in the ERBE observations. In an extended study by Sun et al. (2006), they found that three recent versions of the NCAR Community Atmosphere Model (CAM) continue to overestimate the response of clear-sky greenhouse effect to El Niño warming.

The clear-sky greenhouse effect depends on the water vapor (Zhang and Sun 2006) as well as on the lapse rate (Sun and Lindzen 1993; Held and Soden 2000). Therefore there are two possible causes of the excessive response in the clear-sky greenhouse effect. One is that the response of the water vapor concentration in the troposphere is too strong in the model. The other possibility is that the lapse rate response in the models is not the same as in the observations. We would like to know the relative contributions from these two processes to the excessive response in the clear-sky greenhouse effect noted in the NCAR models. Therefore we examine in this paper the vertical structure of both the water vapor and temperature response to El Niño warming, and we will quantify the contributions from these two factors to the discrepancies seen in the response of the clear-sky greenhouse effect.

2. Methodology, data and model

The clear-sky greenhouse effect (Ga) is defined as the difference between the surface emission and the clear-sky outgoing longwave radiation (OLR) at the top of the atmosphere (see equation (1) of Zhang and Sun (2006)). We employ the same regression analysis of Zhang and Sun (2006) in this study. Note that the regressions involving Ga are conducted for ocean regions only and performed on deseasonalised interannual variations. As we attempt to understand the discrepancy in the clear-sky greenhouse effect between those in the models and that from ERBE (Barkstrom 1984), we again focus on the ERBE period (February 1985 − April 1989).

The clear-sky OLR from the ERBE S-4 data product archived in NCAR Climate and Global Dynamics Division (CGD) is used to calculate the clear-sky greenhouse effect from ERBE observations (see http://www.cgd.ucar.edu/cas/catalog/satellite/erbe/). We adopt the modified monthly mean data in this study that have been reprocessed to accommodate the discontinuity that occurred with the loss of NOAA-9 in January 1987. To avoid the satellite sampling problems and strengthen the conclusions, we also employ the clear-sky OLR data from the National Centers for Environmental Prediction-National Center for Atmospheric Research (NCEP-NCAR) reanalysis (Kalnay et al. 1996) to obtain Ga from NCEP reanalysis.

Observations of cloud cover are obtained from the International Satellite Cloud Climate Project (ISCCP) data (Rossow et al., 1996; Rossow and Schiffer, 1999). The specific humidity, air temperature, and vertical velocity data from NCEP reanalysis are mainly used to examine the model simulations in the present study. To make our

conclusions more robust, we also include the European Centre for Medium-Range Weather Forecasts (ECMWF) reanalyses ERA-40 (Uppala et al., 2005) to evaluate the response of water vapor and temperature from the models. The observed SSTs are from the standard AMIP (Atmospheric Model Intercomparison Project) SST data set at T42 resolution (Gates 1992), the same as those used in many previous studies (Sun and Trenberth 1998; Sun et al. 2003; Sun et al. 2006; Zhang and Sun 2006). The four NCAR models analyzed here are NCAR CCM3 (CAM1), NCAR CAM2, NCAR CAM3 at standard resolution, and NCAR CAM3 at T85. The model data are from the AMIP runs of the four models that have the same SST forcing as observations.

3. Results

Figure 1 shows the spatial pattern of the response of clear-sky greenhouse effect (Ga) in ERBE observations, NCEP reanalysis, and in the models. All the models can simulate the observed positive response from the greenhouse effect of water vapor including the location of the maximum response over the central Pacific, but somewhat overestimate the magnitude of the response. Averaged over the immediate region of El Niño warming (160^oE-290^oE, 5^oS-5^oN), the response of greenhouse effect is 6.37 $Wm^{-2}K^{-1}$ in ERBE observations and 6.84 $Wm^{-2}K^{-1}$ in NCEP data, while the response of Ga in four models is respectively 8.26 $Wm^{-2}K^{-1}$ (CAM1), 8.17 $Wm^{-2}K^{-1}$ (CAM2), 8.33 $Wm^{-2}K^{-1}$ (T42 CAM3) and 8.65 $Wm^{-2}K^{-1}$ (T85 CAM3). So all the models have an excessive response in Ga over

the immediate region of El Niño warming and this excessive response is more severe in the T85 CAM3.

The differences in the response of greenhouse effect between the model simulations and ERBE observations could be in part due to the sampling differences between ERBE and the model data (Zhang et al. 1994; Allan and Ringer 2003; and Sohn et al. 2006), since regional differences in clear-sky OLR due to model-satellite sampling differences can reach 10~15 Wm^{-2}. But the bias due to the inadequate sampling does not explain the large range in the discrepancy as the models also overestimate the response compared to NCEP data (Figure 1). Note that these values presented here are the results of regional response. An early study of Soden (1997) concluded that the response of the tropical mean greenhouse effect of water vapor to El Niño warming in the GFDL model has a close match with that from ERBE observations. We have to note, however, that the tropical mean signal of Ga associated with ENSO is much weaker than the signal averaged over the equatorial cold-tongue region of concern due to cancellations between different regions. The mean response of Ga averaged over the entire domain (120^oE-290^oE, 30^oS-30^oN) is respectively 0.79 $Wm^{-2}K^{-1}$ for ERBE observations, 1.04 $Wm^{-2}K^{-1}$ for CAM1, 0.77 $Wm^{-2}K^{-1}$ for CAM2, 1.00 $Wm^{-2}K^{-1}$ for CAM3 at T42, and 1.17 $Wm^{-2}K^{-1}$ for CAM3 at T85 resolution. So only over the region of immediate warming, all the models overestimate the response of Ga, and the cause of this overestimate is our

concern here. The differences in the drying region will be investigated in a separate paper.

Figure 2 shows the percentage water vapor response at different levels of the troposphere, averaged over the immediate region of El Niño warming (160^{o}E-290^{o}E, 5^{o}S-5^{o}N). In both models and NCEP reanalysis, the response increases with height to about 500-400 mb, then decreases with height further up. (Note that NCEP has no data above 300 mb, so only the response below this level is plotted). The model-data discrepancy in the response of water vapor is small in the low troposphere, but large differences occur in the middle and upper troposphere, where ERA-40 reanalysis gives a quite consistent picture with NCEP data.

Figure 3 further shows a comparison of the vertical profile of the temperature response between two reanalysis data and the models. The discrepancy in the temperature response between models and two reanalysis data at all tropospheric levels is within 0.3 K/K. The maximum discrepancy in the temperature response occurs in the immediate neighborhood of 600 mb. The response of temperature in the middle troposphere is weaker in the models than that from the reanalysis data. The cause for this underestimate in the middle troposphere is that the cold phase is generally warmer in the models than in the reanalysis (not shown here).

To obtain a quantitative measure of the relative contributions to the errors in the clear-sky greenhouse effect from the bias in the response of temperature and the bias in the response of water vapor, we have employed a radiation model (Chou 1986), the same radiation routine used in Sun and Lindzen (1993), to calculate the differences in the greenhouse effect due to different temperature or water vapor profiles. To estimate the contributions from the differences in the lapse rate response to the differences in the clear-sky greenhouse effect response, we first use the annual mean vertical profile of water vapor and temperature from NCEP reanalysis over the region of El Niño warming (160^{o}E-290^{o}E, 5^{o}S-5^{o}N) to calculate the mean clear-sky greenhouse effect as a reference value of Ga. We then add to the reference profiles of temperature the temperature response from NCEP data and models shown in Fig.3, for a 1 K increase in the SST. We keep the water vapor profile fixed unchanged in the calculation of Ga. We then contrast the differences between Ga from the changed temperature profile and Ga from the case with the reference temperature profile. Similarly, to estimate the contributions from the differences in the water vapor response to the differences in the clear-sky greenhouse effect, we keep the temperature profile fixed to the NCEP reference profile, but add to the reference profile for water vapor the response of water vapor for a 1 K increase in the SST (Fig.2). To quantify the combined contributions from the differences in the water vapor response and the differences in the temperature response to the differences in the response of Ga, we add to both profiles of water vapor and temperature their corresponding changes for a 1 K increase in the SST as shown in Fig. 2 and Fig. 3. The

results from these calculations are summarized in Table 1. Nonetheless, we have calculated the relative contributions to the errors in the clear-sky greenhouse effect by using ERA-40 reanalysis as reference profile and obtained the similar results that are also included in Table 1 (see the numbers in parentheses listed in the last three columns of the Table). Clearly, the differences in the water vapor response explain the bulk of the differences in the response of Ga. The contribution from the differences in the temperature response is secondary.

Compared to NCEP reanalysis, in the upper troposphere the models tend to be moister in regions of ascending motion and drier in regions of descending motion. Figure 4 overlays the differences of water vapor between NCEP reanalysis and model simulations (in red and blue) with the vertical velocity (solid and dashed contours) in the models. The figure shows that with exception of the trade wind boundary layer, there are good spatial correlations between the sign of the bias in water vapor and the sign of the mean vertical motion. Both the largest negative bias and the largest positive bias occur around 500-400 hPa where the vertical velocity has its positive/negative maximum. The ascending motion over the western Pacific is generally stronger in the models than in NCEP data. The strength of the vertical motion over the eastern Pacific is more similar between the model simulations and the reanalysis. It thus appears that the dry bias in the model over the region of the descending motion is unlikely due to a stronger mean descending motion. In further reference of the stronger ascending motion in the western Pacific and a much more moist atmosphere in that region, the dry bias in the eastern

pacific is more likely due to a too much concentration of deep convection in the western Pacific or the lack of sufficient eastward excursion of deep convection. Generally, the models have a stronger ascending motion and more moisture compared to NCEP reanalysis in regions with deep convection—the western Pacific warm-pool and the ITCZ (intertropical convergence zone) that is north to the equator in the eastern Pacific.

The models not only have a stronger vertical motion in regions of warm SST, they also have a more sensitive vertical motion to SST change. Figure 5 shows the response of vertical motion to the SST increase in the central Pacific during El Niño warming. Thus, if the stronger motion in the warm-pool region in the mean is a cause of the positive bias of water vapor in the mean (Figure 4), then Figure 5 implies a stronger water vapor response to El Niño warming, which is what we see in Figure 2. Since upward vertical motion is associated with deep moist convection, the picture that is suggested by the analysis here appears to be the following: the deep moist convection in the model has a stronger moistening effect on the free troposphere.

To further quantify the relative contributions to the discrepancy in the water vapor response from the two phases of ENSO, we have performed composite analysis of the water vapor anomaly during the warm and cold phases. The results indicate that the models are not only too moist in the warm periods (Figure 6a) but too dry in the cold periods over the equatorial Pacific cold-tongue region (Figure 6b). The drier bias shown in Fig.4 is thus mainly from the bias in the cold phase. Fig.6cd further shows the

composite of the anomalous vertical motion in the models for the two phases of ENSO. The figures show that the models' vertical motion is more sensitive to El Niño warming (Figure 6c) and to La Niña cooling (Figure 6d) than those in the NCEP reanalysis. The models appear to have a greater bias during the warm phase than in the cold phase. The excessive response of water vapor in the models is also linked to the bias in the response of upper cloud cover (Figure 7a). We have noted that all the models overestimate the upper cloud cover response compared to ISCCP data. The overestimate of water vapor response in the upper troposphere is about 8%/K ~20%/K, and the associated upper cloud cover response is overestimated by about 5%/K in CCM3 and about 3%/K in three latest versions. The response of vertical motion over the region of concern is shown in Figure 7b. The results strengthen the impression that the models have higher sensitivity to SST forcing in the vertical motions in the low and middle troposphere. It is clear that in the NCAR models the excessive response of upper tropospheric water vapor is associated with an excessive response in the vertical motion and upper cloud cover. Further research is needed to establish whether the stronger vertical motion is a cause or a consequence of the excessive upper level cloud amount and humidity.

4. Summary

To better understand the causes of the overestimate in the response of clear-sky greenhouse effect to El Niño warming over the region of warming in four NCAR models,

the response of water vapor and temperature to El Niño warming is examined as a function of height. Consistent with the results from the NCEP reanalysis, all the NCAR models have a stronger water vapor response to the surface ocean warming in the middle to upper troposphere than in the lower troposphere. However, the water vapor response in the middle to upper troposphere in the models is considerably stronger than in the NCEP reanalysis. The temperature response in contrast is weaker in the models in the middle troposphere (the level around 600 mb). The same conclusions are obtained by comparing the model simulations and ERA-40 reanalysis.

Utilizing a radiation model, the data-model discrepancy in the temperature response is found to play a secondary role in giving rise to the bias of greenhouse effect. The difference in the temperature response only accounts for about 10% of the bias in the response of greenhouse effect. The overestimate in the response of greenhouse effect is mostly due to an overestimate of the response in the middle to upper tropospheric water vapor.

Further analysis reveals that compared to the NCEP reanalysis, the excessive response of water vapor in the models is due to the bias that the models are too moist in warm periods and too dry in cold periods. The NCAR models have a stronger vertical motion that is more sensitive to El Niño warming and La Niña cooling than the reanalysis, suggesting a positive correlation between vertical motion and water vapor. Also, the response of upper cloud cover is overestimated in all the models. Further research is needed to establish whether the stronger vertical motion is a consequence or a cause of

the higher upper cloud cover and the excessive upper level humidity in the models.

Consistent with earlier analysis (Sun et al. 2001), the correlation between the upper tropospheric humidity variations and those at the surface level over the tropics is found to be higher in the NCAR models than in the reanalysis (Not shown). Therefore a possible excessive background diffusion in the models continues to be a concern. All the NCAR models use the Zhang and McFarlane (1995) parameterization for deep moisture convection and they have a stronger ascending motion in the deep convection regions. Whether the stronger vertical motion is due to the deep convection scheme used needs to be further investigated. We also note that in the middle troposphere, two CAM3 models have a comparable cloud response to El Niño warming but they have an excessive water vapor response (the overestimate is about 20%/K). Interestingly, for the other two models, the water vapor response is also considerably larger in the middle troposphere but the middle cloud response is apparently underestimated. This again highlights the fact that we do not yet know well the relationship between clouds and humidity, and more generally the precipitation efficiency of tropical convection. With new satellite data from "A Train" (Stephens et al. 2002), we may be in a better position to address these critical climate issues.

Acknowledgement

This research was supported by NOAA's Climate Dynamics and Environmental Prediction Program, and by NSF's climate dynamics program under ATM-9912434, ATM-0332760, and ATM 0553111. The authors would like to thank Dr. James J. Hack and Dr. Jeff Kiehl of NCAR for providing us the outputs from T85 CAM3.

References

Allan, R. P., and M. A. Ringer, 2003: Inconsistencies between satellite estimates of longwave cloud forcing and dynamical fields from reanalyses, *Geophys. Res. Lett.*, 30(9), 1491, doi:10.1029/2003GL017019.

Barkstrom, B. R., 1984: The Earth Radiation Budget Experiment (ERBE), *Bull. Am. Meteorol. Soc.*, *65*, 1170–1185.

Boer G. J., B. Yu, S.-J. Kim, and G. M. Flato, 2004: Is there observational support for an El Niño-like pattern of future global warming? *Geophys. Res. Lett.*, **31**, L06201, doi:10.1029/2003GL018722.

Cai W., and P. H. Whetton, 2000: Evidence for a time-varying pattern of greenhouse warming in the Pacific Ocean. *Geophys. Res. Lett.*, **27**, 2577–2580.

Chou, M. D., 1986: Atmospheric solar heating rate in water vapour bands. *J. Climate Appl. Meteor.,* **25**, 1532-1542.

Gates, W. L., 1992: AMIP: The Atmospheric Model Intercomparison Project. *Bull. Amer. Meteor. Soc.,* **73,** 791–794.

Held, I. M. and B. J. Soden, 2000: Water vapor feedback and global warming. *Ann. Rev. Energy Environ*., **25**, 441-475.

Houghton J. T., Y. Ding, D. J. Griggs, M. Noguer, P. J. van der Linden, X. Dai, K. Maskell, and C. A. Johnson, 2001: *Climate Change 2001: The Scientific Basis*. Cambridge University Press, 881 pp.

Kiehl, J. T., and K. E. Trenberth, 1997: Earth's annual global mean energy budget. *Bull. Amer. Meteor. Soc.,* **78**, 197–208.

Kalnay, E., and Coauthors, 1996: The NCEP/NCAR 40-Year Reanalysis Project. *Bull. Amer. Meteor. Soc.,* **77**, 437–471.

Meehl G. A., and W. M. Washington, 1996: El Niño-like climate change in a model with increased atmospheric CO_2 concentrations. *Nature*, **382**, 56–60.

Rossow, W. B., and R. A. Schiffer, 1999: Advances in understanding clouds from ISCCP, Bull. Am. Meteorol. Soc., 80, 2261–2288.

Rossow, W. B., A. W. Walker, D. E. Beuschel, and M. D. Roiter, 1996: International Satellite Cloud Climatology Project (ISCCP) documentation of new cloud datasets, Rep. WMO/TD-737, 115 pp., World Meteorol. Organ., Geneva, Switzerland.

Soden, B. J.**,** 1997: Variations in the tropical greenhouse effect during El Niño, *J. Clim.*, **10**, 1050–1055.

Sohn, B.-J., J. Schmetz, R. Stuhlmann, and J.-Y. Lee, 2006: Dry Bias in Satellite-Derived Clear-Sky Water Vapor and Its Contribution to Longwave Cloud Radiative Forcing, *J. Clim.*, **19**, 5570–5580.

Stephens G. L, Coauthors, 2002: The Cloudsat Mission and the A-Train. *Bull. Amer. Meteor. Soc.*, **83**, 1771–1790.

Stocker, T. F., and Coauthors, 2001: Physical climate processes and feedbacks. *Climate Change 2001: The Scientific Basis* (Contribution of Working Group I to the Third

Assessment Report of the Intergovernmental Panel on Climate Change). J. T. Houghton et al., Eds., Cambridge University Press, 417-470.

Sun, D.-Z., and R. S. Lindzen, 1993: Water vapor feedback and the ice age snowline record. *Ann. Geophys.*, **11**, 204-215.

Sun D.-Z., and I. Held, 1996: A comparison of modeled and observed relationships between interannual variations of water vapor and temperature. *J. Climate*, **9**, 665–675.

Sun, D.-Z., and K. E. Trenberth, 1998: Coordinated heat removal from the equatorial Pacific during the 1986–87 El Niño, Geophys. Res. Lett., 25, 2659–2662.

Sun, D.-Z., C. Covey, and R. S. Lindzen, 2001: Vertical correlations of water vapor in GCMs, *Geophys. Res. Lett.*, *28*, 259–262.

Sun, D.-Z., J. Fasullo, T. Zhang, and A. Roubicek, 2003: On the radiative and dynamical feedbacks over the equatorial cold-tongue. *J. Clim.*, **16**, 2425-2432.

Sun, D.-Z., T. Zhang, C. Covey, S. A. Klein, W. D. Collins, J. J. Hack, J. T. Kiehl, G. A. Meehl, I. M. Held, and M. Suarez, 2006: Radiative and Dynamical Feedbacks Over the Equatorial Cold-tongue: Results from Nine Atmospheric GCMs. *J. Clim.*, **19**, 4059-4074.

Timmerman A. J., J. Oberhuber, A. Bacher, M. Esch, M. Latif, and E. Roeckner, 1999: Increased El Niño frequency in a climate model forced by future global warming. *Nature*, **398**, 694–696.

Uppala, S. M., et al., 2005: The ERA-40 reanalysis, Q. J. R. Meteorol. Soc., 131, 2961–3012, doi:10.1256/qj.04.176/.

Zhang, G. J., and N. A. McFarlane, 1995: Sensitivity of climate simulations to the parameterization of cumulus convection in the Canadian Climate Centre general circulation model, Atmos. Ocean., 33, 407–446.

Zhang M. H., R. D. Cess, T. Y. Kwon, and M. H. Chen, 1994: Approaches of comparison for clear-sky radiative fluxes from general circulation models with Earth Radiation Budget Experiment data. *J. Geophys. Res.*, **99**, 5515–5523.

Zhang, T. and D.-Z. Sun, 2006: Response of water vapor and clouds to El Niño warming in three National Center for Atmospheric Research atmospheric Models. *J. Geophys. Res.*, **111**, D17103, doi:10.1029/2005JD006700.

Table captions

Table 1: The discrepancy with ERBE observations and NCEP reanalysis (the numbers in parentheses) in the response of clear-sky greenhouse effect (Ga) and the contributions to this discrepancy due to the errors in temperature and humidity response in NCAR models with respect to NCEP reanalysis over the region of El Niño warming (160^{o}E-290^{o}E, 5^{o}S-5^{o}N). The contributions to Ga discrepancy are calculated as the differences in the response of Ga to 1K SST increase between models and the same NCEP reference value for each case (see text for details). The numbers in parentheses listed in the last three columns of the table are the contributions to Ga discrepancy estimated from the results using ERA-40 reanalysis as reference value.

Figure captions

Figure 1: Response of the clear-sky greenhouse effect (Ga) to El Niño warming from (a) ERBE observations, (b) NCEP reanalysis, (c) CAM1, (d) CAM2, (e) T42 CAM3, and (f) T85 CAM3. Shown are regression coefficients obtained by linearly regressing the clear-sky greenhouse effect at each grid point against the underlying SST averaged over the region of El Niño warming (160^{o}E-290^{o}E, 5^{o}S-5^{o}N). The interannual variations of Ga over the ERBE period are used for the calculations.

Figure 2: Percentage response of specific humidity to El Niño warming as a function of height from the NCEP-NCAR reanalysis, ERA-40 reanalysis, and four NCAR models averaged over the equatorial Pacific (160^{o}E-290^{o}E, 5^{o}S-5^{o}N). Shown are regression coefficients divided by the respective climatology. In every vertical level, the regression coefficients are obtained by linearly regressing specific humidity at the corresponding level against the underlying SST (as in Figure 19 of Zhang and Sun [2006]) averaged over the region of El Niño warming (160^{o}E-290^{o}E, 5^{o}S-5^{o}N). The interannual variations of specific humidity over the ERBE period are used for the regression calculations.

Figure 3: Response of air temperature to El Niño warming as a function of height from

the NCEP-NCAR reanalysis, ERA-40 reanalysis, and four NCAR models averaged over the equatorial Pacific (160^{o}E-290^{o}E, 5^{o}S-5^{o}N). Shown in every vertical level are regression coefficients obtained by linearly regressing the air temperature at the corresponding level against the underlying SST averaged over the region of El Niño warming (160^{o}E-290^{o}E, 5^{o}S-5^{o}N). The interannual variations of air temperature over the ERBE period are used for the regression calculations.

Figure 4: The vertical cross sections averaged over the equator (5^{o}S-5^{o}N) (left panel) and spatial patterns at 400 hPa (right panel) for annual mean vertical velocity over the ERBE period from NCEP reanalysis and four models. Note that the negative contour lines indicate the ascending motions and the positive contour lines indicate the descending motions. The shaded values in (b-e) and (g-j) are the percentage differences in annual mean specific humidity between the models and NCEP data over the same period. They are obtained from the differences between models and NCEP data divided by the values of NCEP data.

Figure 5: The spatial pattern of the response of vertical velocity to El Niño warming at 850 hPa (left panel) and at 500 hPa (right panel) from the NCEP-NCAR reanalysis and four NCAR models. Shown are regression coefficients obtained by linearly regressing vertical velocity against the underlying SST averaged over the region of El Niño warming (160^{o}E-290^{o}E, 5^{o}S-5^{o}N). The interannual variations of vertical velocity over the

ERBE period are used for the regression calculations.

Figure 6: The composite percentage changes in specific humidity during (a) warm periods and (b) cold periods as a function of height from the NCEP-NCAR reanalysis and four NCAR models averaged over the equatorial Pacific (160^{o}E-290^{o}E, 5^{o}S-5^{o}N). The percentage changes in specific humidity are calculated as the anomalies divided by the respective climatology. Also shown are the composite changes in vertical velocity during (c) warm periods and (d) cold periods as a function of height from the NCEP-NCAR reanalysis and four NCAR models averaged over the equatorial Pacific (160^{o}E-290^{o}E, 5^{o}S-5^{o}N). The warm and cold periods are defined as the periods when the Niño-3 SST anomalies are larger than 0.3^{o}C and less than -0.3^{o}C over the ERBE period, respectively.

Figure 7: Responses of (a) cloud cover from ISCCP observations and four models, and (b) vertical velocity from the NCEP reanalysis and four models to El Niño warming as a function of height averaged over the equatorial Pacific (160^{o}E-290^{o}E, 5^{o}S-5^{o}N). The cloud cover data used here are the high, middle and low cloud cover for both models and observations, the same as those used by Sun et al. (2003) and Zhang and Sun (2006). Shown in every vertical level are regression coefficients obtained by linearly regressing the concerned quantities at the corresponding level against the underlying SST averaged over the region of El Niño warming (160^{o}E-290^{o}E, 5^{o}S-5^{o}N). The interannual variations of the concerned quantities over the ERBE period are used for the regression calculations.

Table 1: The discrepancy with ERBE observations and NCEP reanalysis (the numbers in parentheses) in the response of clear-sky greenhouse effect (Ga) and the contributions to this discrepancy due to the errors in temperature and humidity response in NCAR models with respect to NCEP reanalysis over the region of El Niño warming (160^oE-290^oE, 5^oS-5^oN). The contributions to Ga discrepancy are calculated as the differences in the response of Ga to 1K SST increase between models and the same NCEP reference value for each case (see text for details). The numbers in parentheses listed in the last three columns of the table are the contributions to Ga discrepancy estimated from the results using ERA-40 reanalysis as reference value.

Model Names	Ga discrepancy with ERBE and NCEP ($Wm^{-2}K^{-1}$)	contribution to the discrepancy ($Wm^{-2}K^{-1}$)		
		Lapse rate effect	Humidity effect	combined effect
CAM1	1.89 (1.42)	0.053 (0.071)	1.65 (1.48)	1.71 (1.56)
CAM2	1.80 (1.33)	0.31 (0.36)	0.87 (0.43)	1.21 (0.81)
CAM3	1.96 (1.49)	0.23 (0.27)	1.12 (0.74)	1.39 (1.04)
CAM3 (T85)	2.28 (1.81)	0.020 (0.039)	1.66 (1.40)	1.70 (1.46)

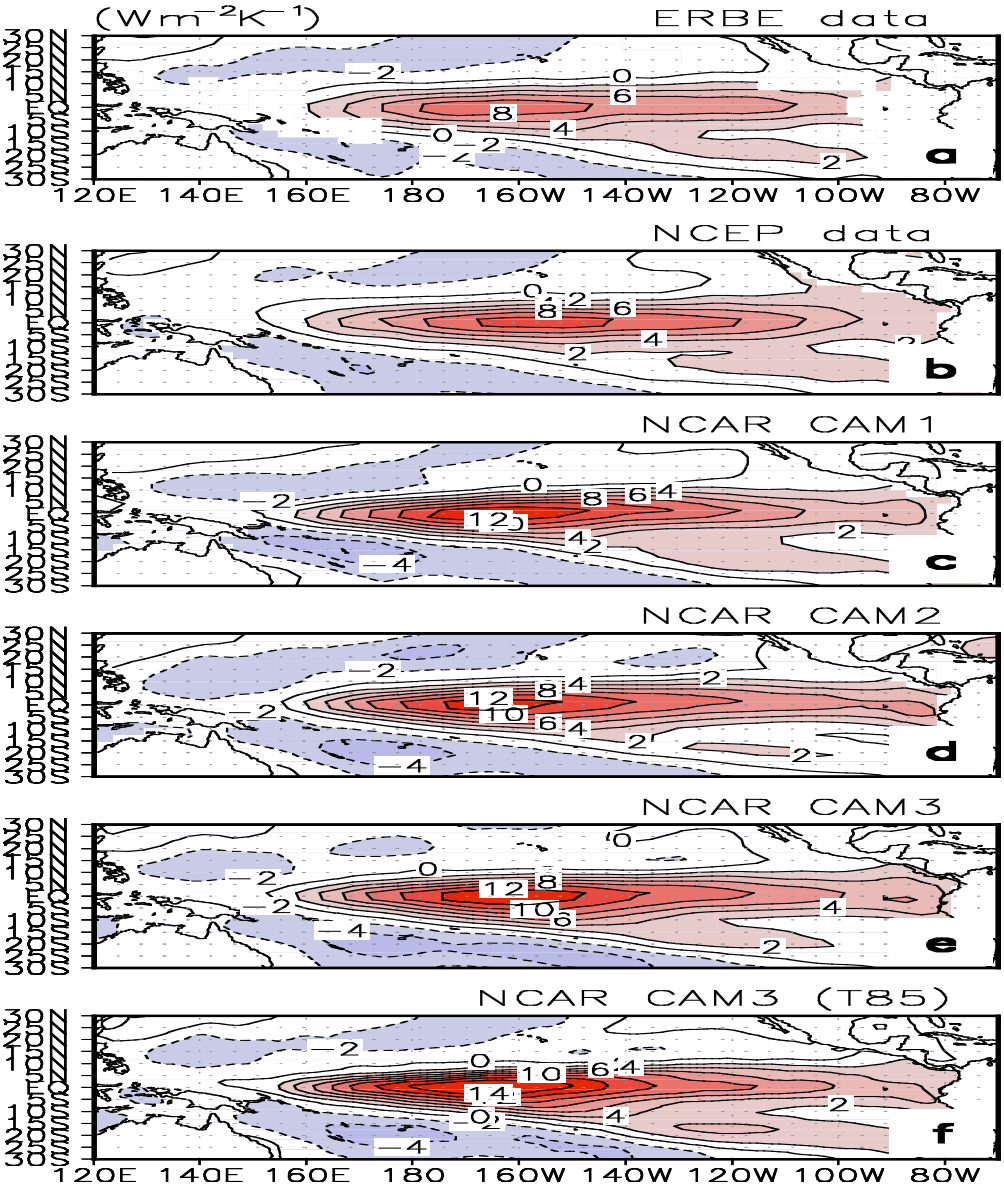

Figure 1: Response of the clear-sky greenhouse effect (Ga) to El Niño warming from (a) ERBE observations, (b) NCEP reanalysis, (c) CAM1, (d) CAM2, (e) T42 CAM3, and (f) T85 CAM3. Shown are regression coefficients obtained by linearly regressing the clear-sky greenhouse effect at each grid point against the underlying SST averaged over the region of El Niño warming (160°E-290°E, 5°S-5°N). The interannual variations of Ga over the ERBE period are used for the calculations.

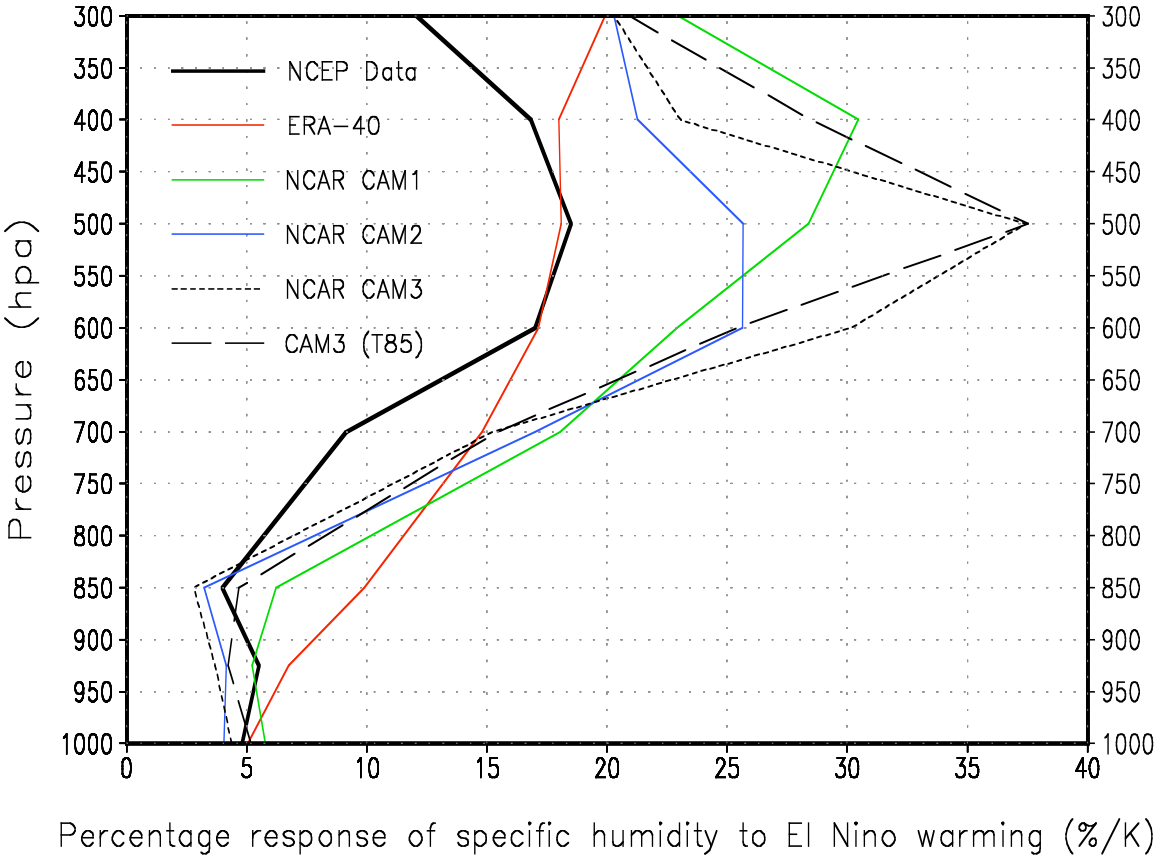

Figure 2: Percentage response of specific humidity to El Niño warming as a function of height from the NCEP-NCAR reanalysis, ERA-40 reanalysis, and four NCAR models averaged over the equatorial Pacific (160°E-290°E, 5°S-5°N). Shown are regression coefficients divided by the respective climatology. In every vertical level, the regression coefficients are obtained by linearly regressing specific humidity at the corresponding level against the underlying SST (as in Figure 19 of Zhang and Sun [2006]) averaged over the region of El Niño warming (160°E-290°E, 5°S-5°N). The interannual variations of specific humidity over the ERBE period are used for the regression calculations.

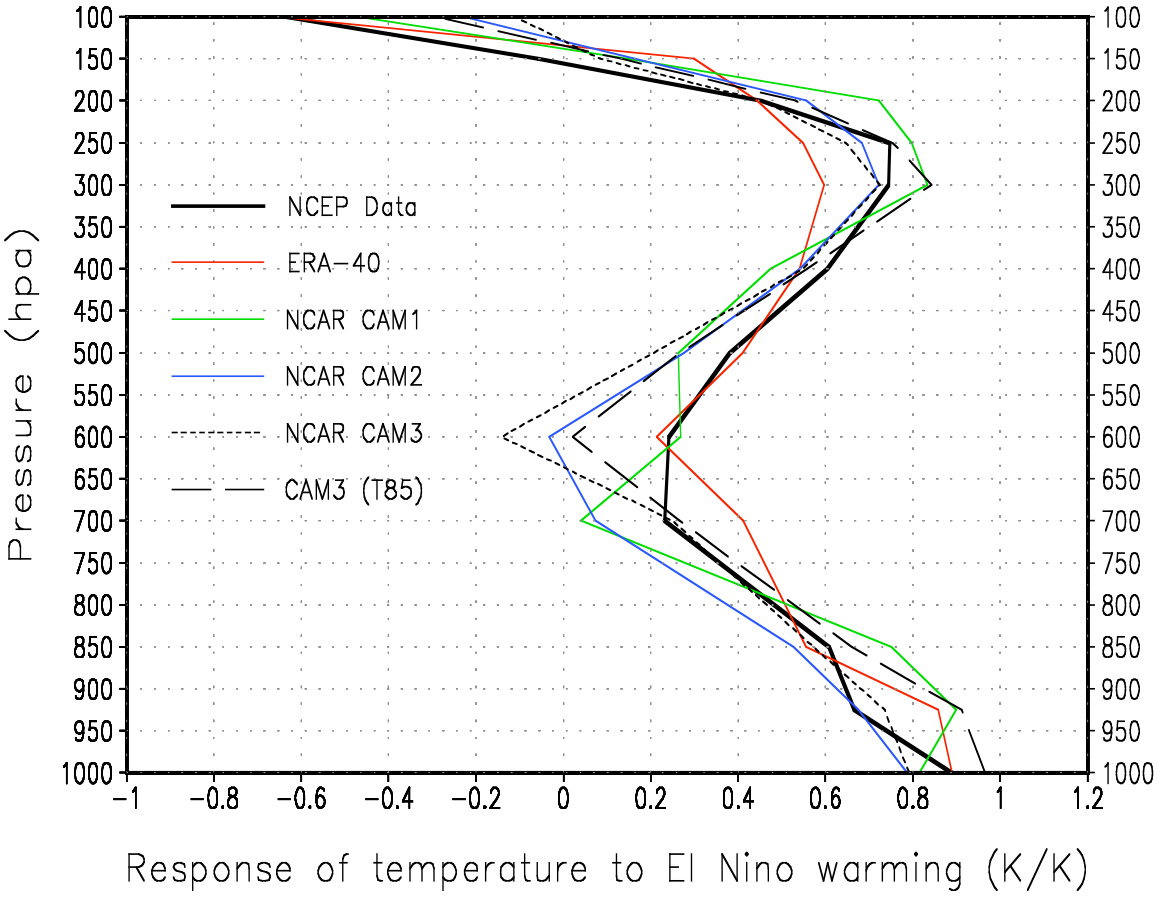

Figure 3: Response of air temperature to El Niño warming as a function of height from the NCEP-NCAR reanalysis, ERA-40 reanalysis, and four NCAR models averaged over the equatorial Pacific (160°E-290°E, 5°S-5°N). Shown in every vertical level are regression coefficients obtained by linearly regressing the air temperature at the corresponding level against the underlying SST averaged over the region of El Niño warming (160°E-290°E, 5°S-5°N). The interannual variations of air temperature over the ERBE period are used for the regression calculations.

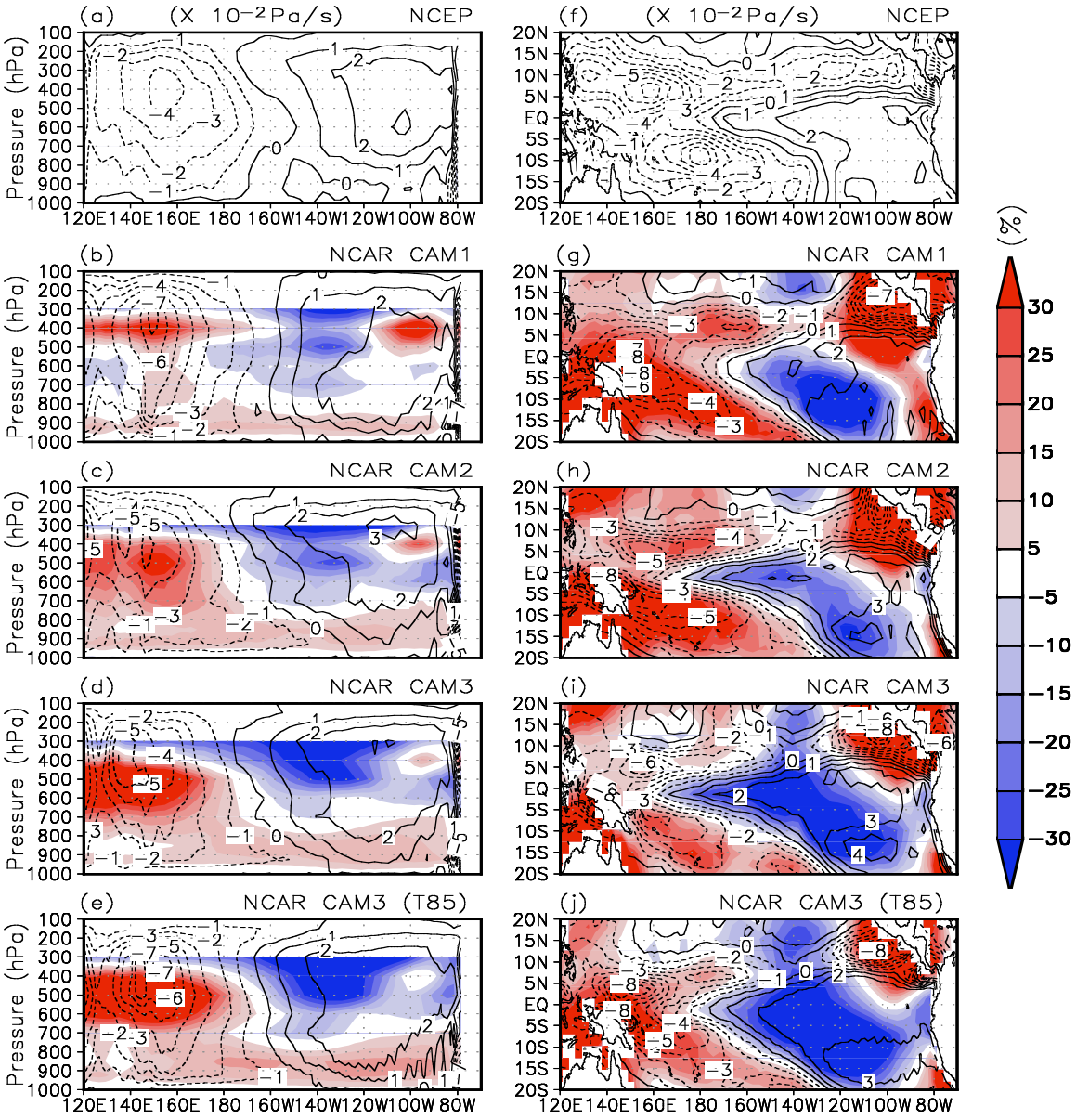

Figure 4: The vertical cross sections averaged over the equator (5°S-5°N) (left panel) and spatial patterns at 400 hPa (right panel) for annual mean vertical velocity over the ERBE period from NCEP reanalysis and four models. Note that the negative contour lines indicate the ascending motions and the positive contour lines indicate the descending motions. The shaded values in (b-e) and (g-j) are the percentage differences in annual mean specific humidity between the models and NCEP data over the same period. They are obtained from the differences between models and NCEP data divided by the values of NCEP data.

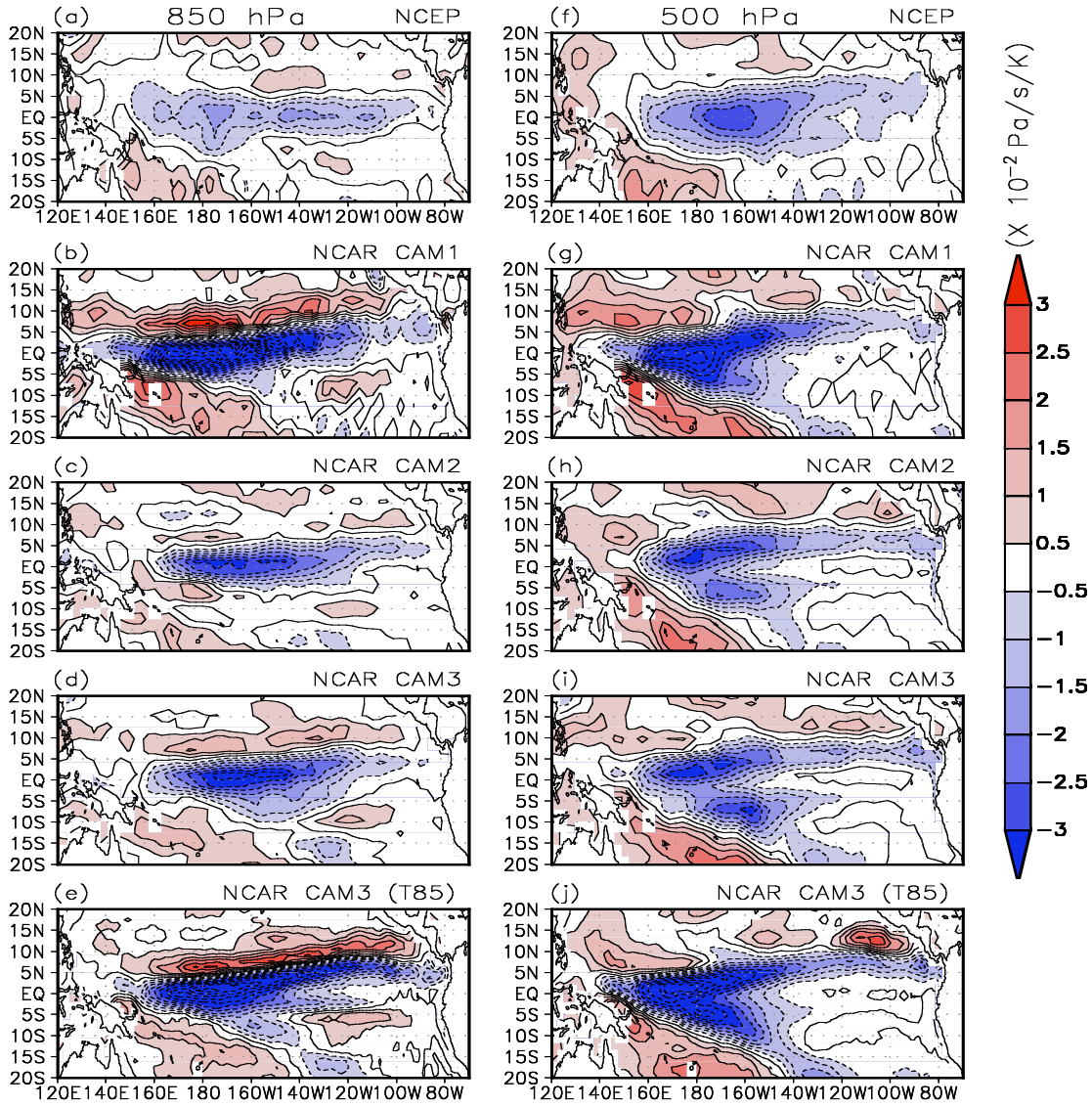

Figure 5: The spatial pattern of the response of vertical velocity to El Niño warming at 850 hPa (left panel) and at 500 hPa (right panel) from the NCEP-NCAR reanalysis and four NCAR models. Shown are regression coefficients obtained by linearly regressing vertical velocity against the underlying SST averaged over the region of El Niño warming (160^{o}E-290^{o}E, 5^{o}S-5^{o}N). The interannual variations of vertical velocity over the ERBE period are used for the regression calculations.

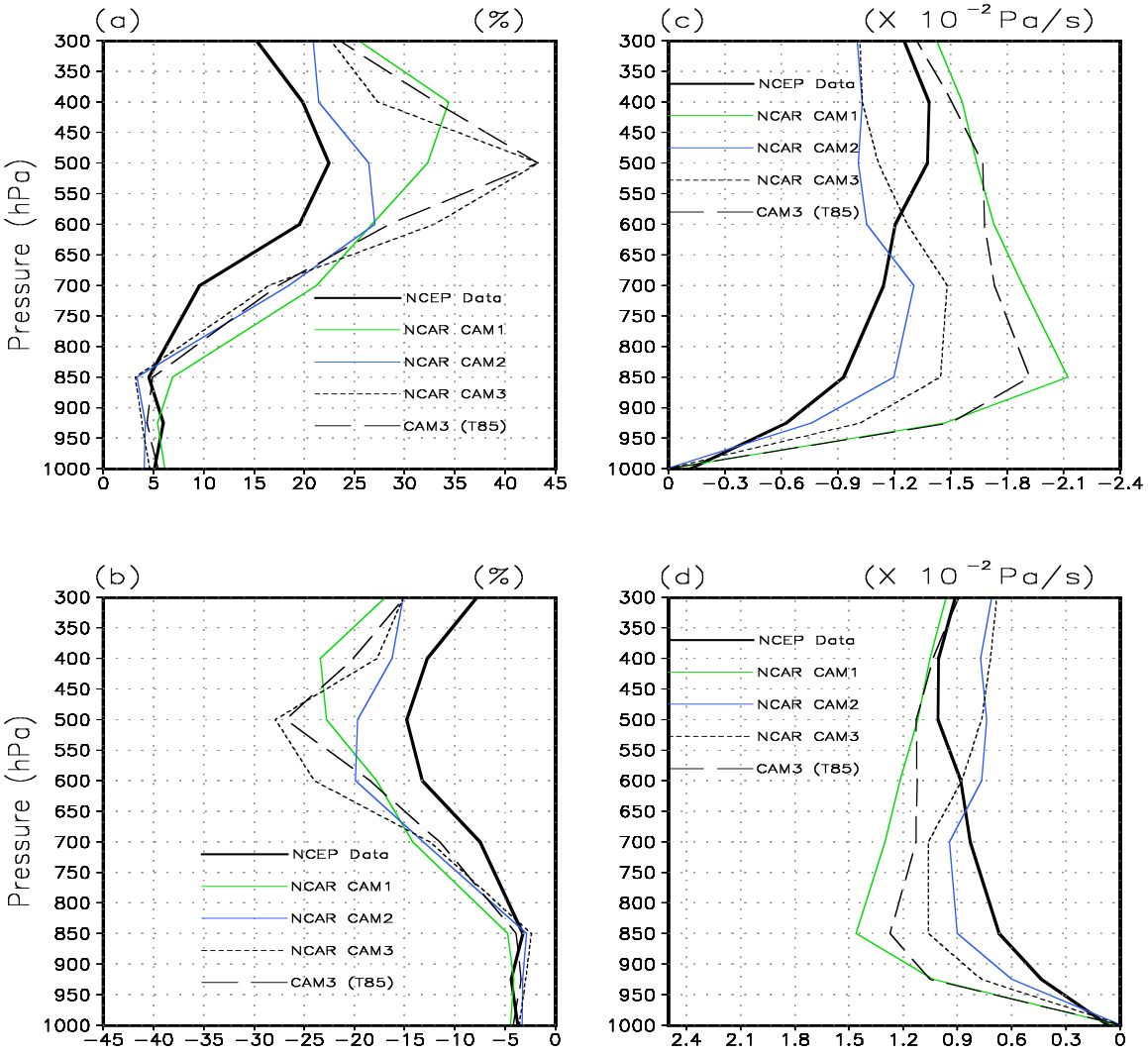

Figure 6: The composite percentage changes in specific humidity during (a) warm periods and (b) cold periods as a function of height from the NCEP-NCAR reanalysis and four NCAR models averaged over the equatorial Pacific (160°E-290°E, 5°S-5°N). The percentage changes in specific humidity are calculated as the anomalies divided by the respective climatology. Also shown are the composite changes in vertical velocity during (c) warm periods and (d) cold periods as a function of height from the NCEP-NCAR reanalysis and four NCAR models averaged over the equatorial Pacific (160°E-290°E, 5°S-5°N). The warm and cold periods are defined as the periods when the Niño-3 SST anomalies are larger than 0.3°C and less than -0.3°C over the ERBE period, respectively.

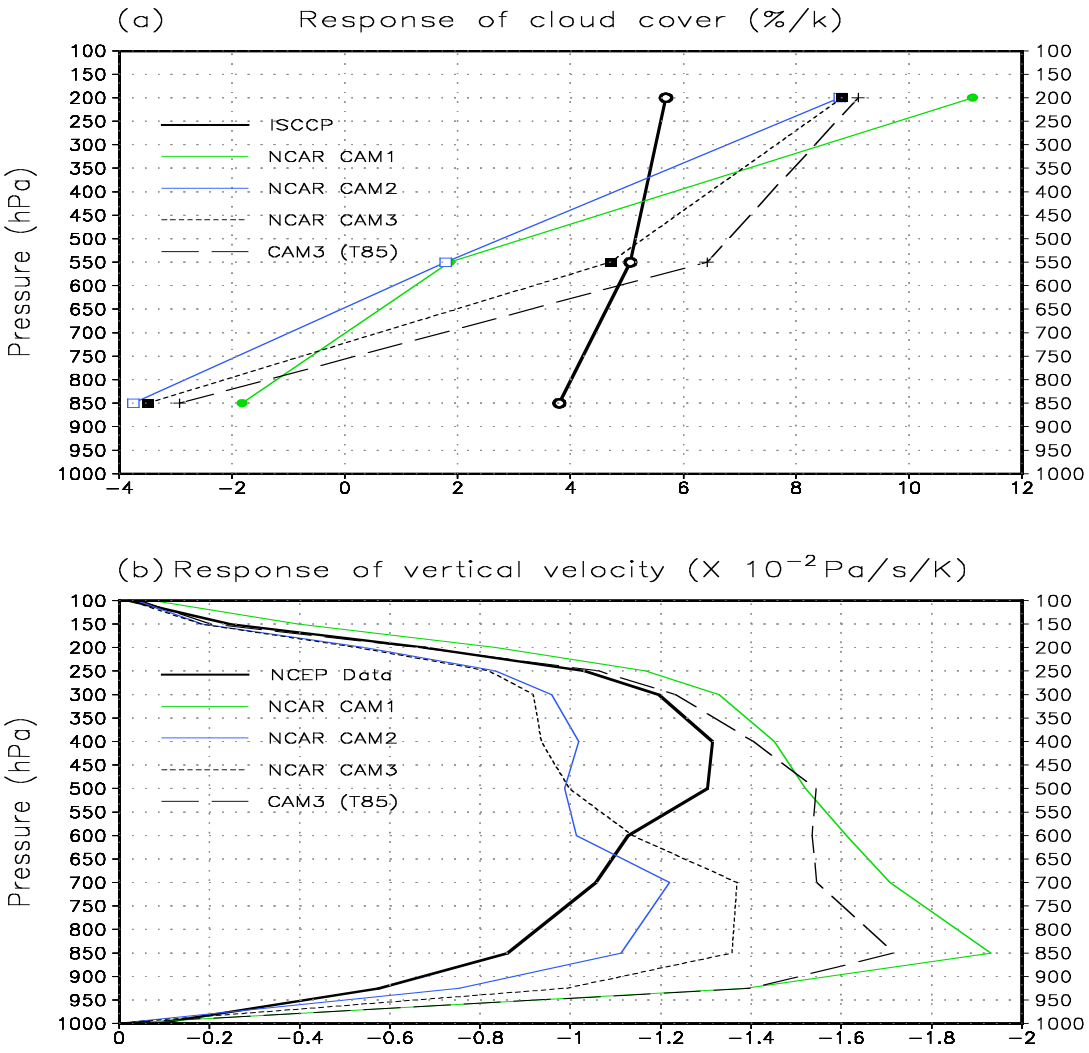

Figure 7: Responses of (a) cloud cover from ISCCP observations and four models, and (b) vertical velocity from the NCEP reanalysis and four models to El Niño warming as a function of height averaged over the equatorial Pacific (160°E-290°E, 5°S-5°N). The cloud cover data used here are the high, middle and low cloud cover for both models and observations, the same as those used by Sun et al. (2003) and Zhang and Sun (2006). Shown in every vertical level are regression coefficients obtained by linearly regressing the concerned quantities at the corresponding level against the underlying SST averaged over the region of El Niño warming (160°E-290°E, 5°S-5°N). The interannual variations of the concerned quantities over the ERBE period are used for the regression calculations.